The size of the accretion region in intermediate polars: eclipses of XY Arietis observed with *RXTE*

Coel Hellier

Department of Physics, Keele University, Keele, Staffordshire, ST5 5BG

ABSTRACT

RXTE observed 20 eclipse egresses of the intermediate polar XY Ari in order to study the size and structure of the X-ray emitting accretion regions. The spin-phase averaged egress lasts 26 s, implying a white dwarf radius of 4.3–7.0×10^8 cm. The individual egresses occur later in orbital phase with later spin phase, as expected if the white dwarf spins in the same sense as the orbital motion. The eclipse times trace out the motion of the upper pole across the white dwarf face; then, when the upper pole disappears over the white dwarf limb and the lower pole appears, they trace the motion of the lower pole across the face.

Aligning all the egresses shows that the majority of the X-ray flux emerges in < 2 s, implying accretion regions with area, f, < 0.002 as a fraction of the white dwarf surface. Using only the spin-phase to align the egresses, however, gives a longer (~ 5 s) time for the emergence of the majority of the flux, implying that the accretion regions wander over an area of $f < 0.01$. There is also evidence that a minority of the flux emerges from a much larger area, or that we see accretion regions at both poles simultaneously at some spin phases.

Key words: accretion, accretion discs – novae, cataclysmic variables – binaries: close – binaries: eclipsing – stars: individual: XY Ari – X-rays: stars.

1 INTRODUCTION

If a close binary system is eclipsing it is far easier to obtain constraints on the geometry of the binary. The 206-s X-ray pulsar XY Ari (H0253+193) might have seemed destined to obscurity by its location behind the molecular cloud Lynds 1457, since the optical flux is extinguished to $V > 23$. However, following Patterson & Halpern's (1990) suggestion that it was an intermediate polar (IP – a magnetic white dwarf accreting material from a close companion), Kamata, Tawara & Koyama (1991) discovered deep X-ray eclipses recurring with a 6.06-h orbital period. XY Ari is now the only known IP with a deep X-ray eclipse (EX Hya shows a partial X-ray eclipse while DQ Her shows a deep eclipse but negligible X-ray flux; see Patterson 1994 for a review of these stars).

The identification of XY Ari in the infra-red (Zuckerman et al. 1993) allows modelling of the ellipsoidal variations in the light curve (Allan, Hellier & Ramseyer 1996), tying down the system parameters. Kamata & Koyama (1993) made the first attempt to use the X-ray eclipse to constrain the accretion geometry, using 5 ingresses and egresses observed with *Ginga*. They concluded that the time of ingress/egress was comparable to the expected size of the

white dwarf, and showed the potential of observing more eclipses at a higher count rate.

Accordingly, I proposed an observation of 20 eclipse egresses with the larger PCA on the *RXTE* satellite (Bradt, Rothschild & Swank 1993). The aim was to record changes of the eclipse egress with the phase of the 206-s white dwarf spin cycle. I chose to observe only egresses so that they were all directly comparable: at ingress the secondary star limb is at a different angle on the white dwarf, potentially providing more information, but requiring more eclipses to look for patterns.

The motivation for the observations is that after 15 years of studying IPs there is no agreement on the pattern of accretion flow onto the white dwarf, with estimates of f, the fraction of the white dwarf onto which accretion occurs, differing by orders of magnitude. King & Shaviv (1984), Norton & Watson (1989) and Patterson (1994) all argue for $f > 0.1$–0.3; while Rosen, Mason & Cordova (1988), Hellier, Cropper & Mason (1991) and Hellier (1995) claim $f = 0.01$–0.001. This paper presents direct geometric evidence addressing this issue.
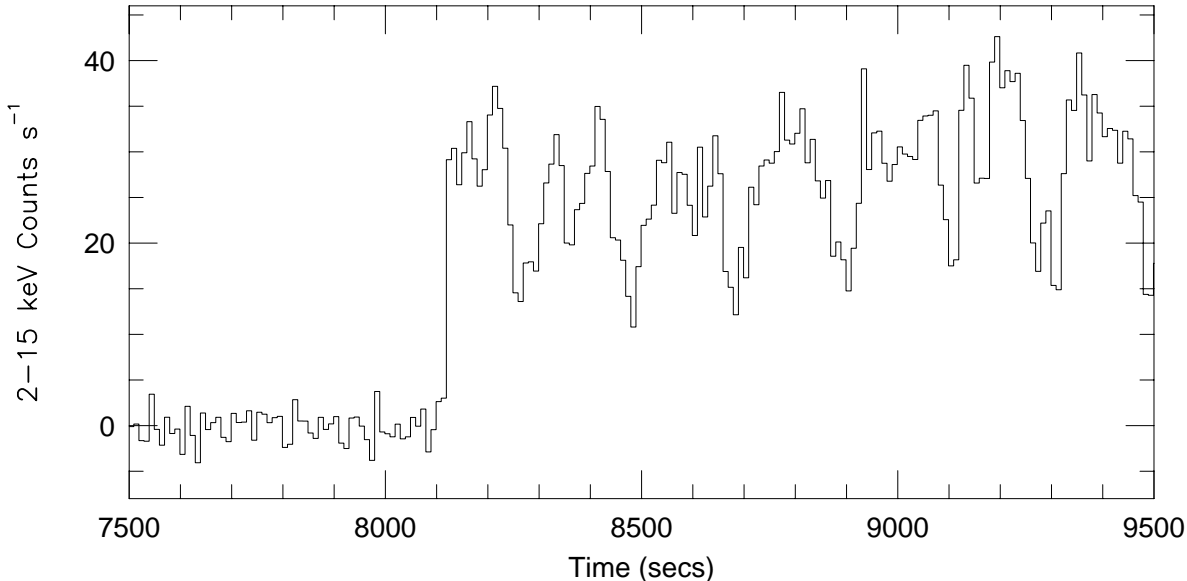
Figure 1. One of the 20 *RXTE* lightcurves of XY Ari, showing the star emerging from eclipse and pulsing at the 206-s spin period. Each bin lasts 10 s. The errors can be judged from the data in eclipse, since the high background level means that photon noise is nearly constant.

2   OBSERVATIONS

The 20 eclipse egresses were observed by *RXTE* over the period 1996 July 13 to 1996 August 11, at a rate of roughly one per day. Each observation lasted ~ 2000 s, with the first 1000 s in eclipse and the later half covering ~ 5 spin cycles. As a bonus XY Ari went into outburst during this period, giving 14 observations in quiescence and 6 in outburst. The outburst is discussed in a companion paper (Hellier, Mukai & Beardmore 1997), while this paper concentrates on the eclipse.

I extracted lightcurves in the energy range 2–15 keV, using data from the top Xenon layer of the PCA only [this gives a higher signal-to-noise ratio (S/N) for dim sources]. I then subtracted the background estimated using PCABACK-EST v1.4f. This marginally underestimated the count rate in eclipse, so I fitted a line to the data in eclipse and subtracted that as a final tweak. The best lightcurve (the one with the egress occurring at the highest count rate) is shown in Fig. 1. Further lightcurves appear in Hellier et al. (1997). All times were converted to barycentric dynamical time.

In quiescence the X-ray spin pulse of XY Ari has a low amplitude (~ 25 per cent) and is double-peaked (e.g. Kamata & Koyama 1993). Fig. 2 shows the Fourier transform of the 14 quiescent observations around the first harmonic of the spin pulse. Since the observations are so short compared to the data gaps the aliasing is severe, but fortunately the *Ginga* spin period of 206.298 s (Kamata et al. 1991) selects the correct alias and agrees well with the current data.

3   THE ECLIPSE EGRESSES

I first folded all 20 lightcurves on the orbital ephemeris of Allan et al. (1996), and show the 'averaged' egress in Fig. 3. To measure the times and length of egress I fitted the data with two constants, one for the eclipsed light and one for
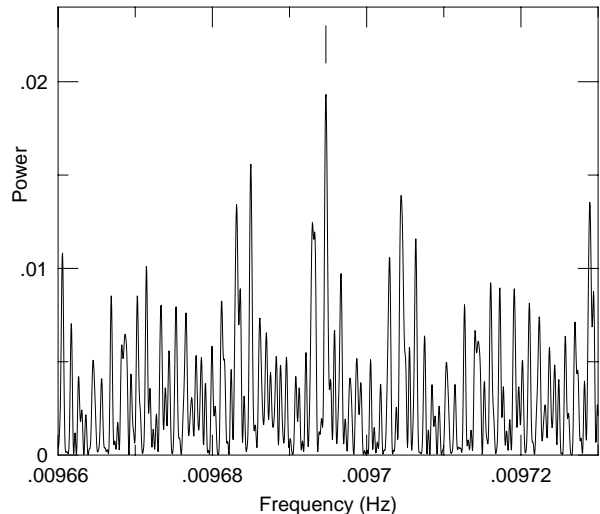

Figure 2. The Fourier transform of the 14 quiescent observations of XY Ari. The tick mark locates the first harmonic of the 206.298-s spin pulse.

the uneclipsed light, and joined these by a straight line of variable slope. The best-fitting eclipse egress lasted 25.8 s ($^{+1.5}_{-1.8}$ at 68 per cent confidence and $^{+3.5}_{-4.2}$ at 90 per cent confidence), while the phase of mid-egress was 0.0546(1).[*] The start of egress ($3^{\rm rd}$ contact) is very well defined but the end is rounded, introducing most of the uncertainty. In fact

---

[*] Warning: since I have no eclipse ingresses I can't estimate the absolute orbital phase reliably, and so use the Allan et al. (1996) ephemeris throughout. However, comparison with the length of the *Ginga* eclipse suggests that this ephemeris has accumulated a phase error of 0.0077, which should be subtracted from any phases to give a better estimate of the absolute value.
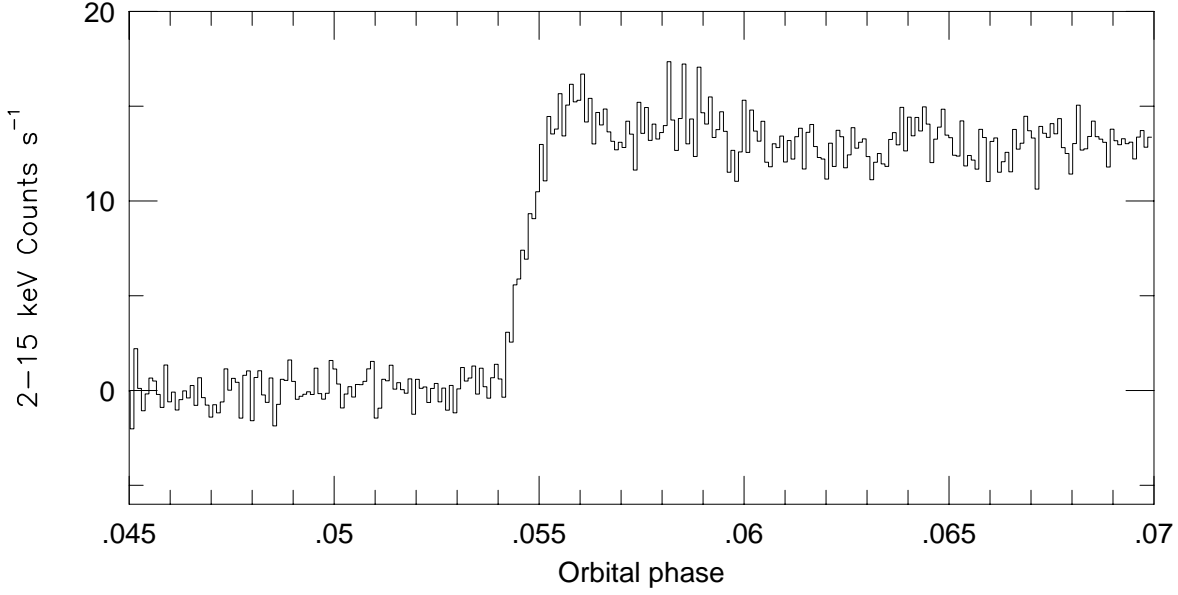
Figure 3. The averged eclipse egress of XY Ari. Each bin lasts 2 s. Third contact occurs at TDB 245 0278.82050(1).
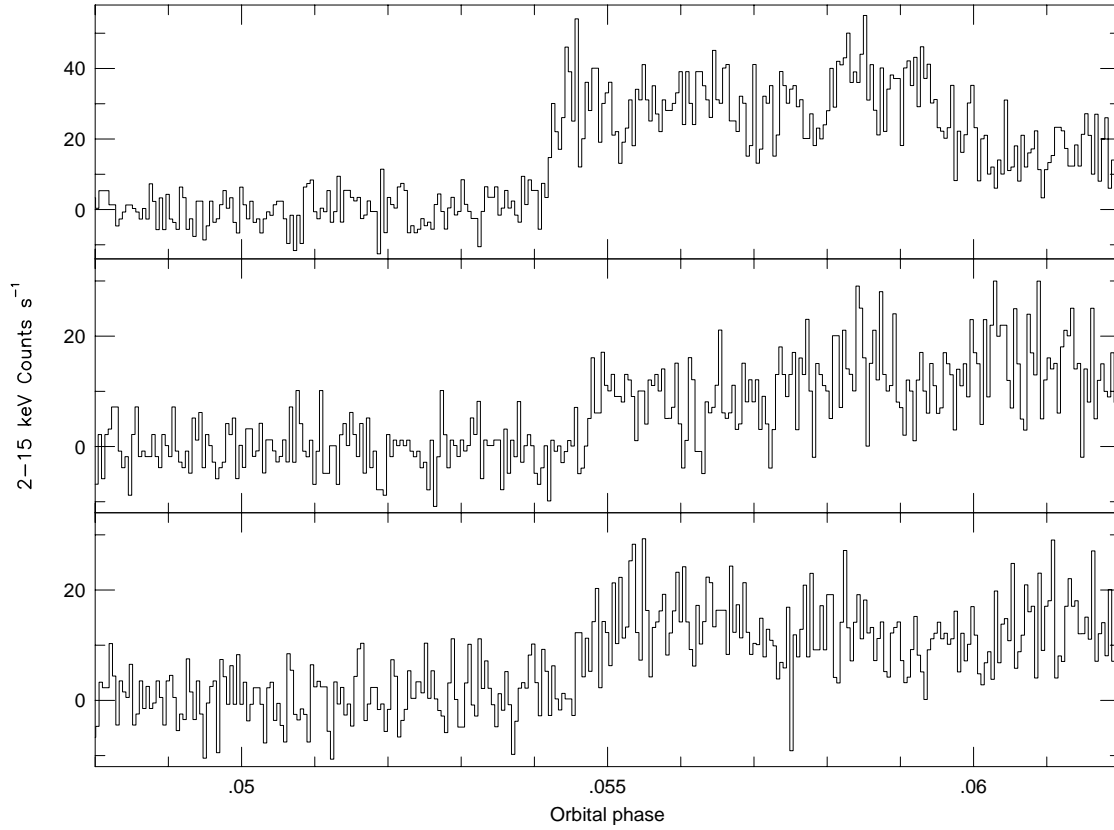

Figure 4. Three of the 20 egresses, shown at 1-s resolution. The uppermost egress is that from Fig. 1, shown at a higher time resolution. As can be seen, the egresses occur at different orbital phases.

the star appears ~ 2 counts s^{-1} brighter immediately after egress and also slightly brighter just before egress (although the latter is not statistically significant). The post-egress brightening (if it is flickering) would tend to bias the egress measurement to a greater duration. If the brightenings are not flickering they might be explainable by X-rays scattered in the corona of the secondary star into the line of sight.

The egress in Fig. 3 is the average over spin phase, so the length of egress depends on the size of the tracks over which accretion can occur through the spin cycle, rather than on the size of the accretion region at any one time. To investigate that we need to look at the individual eclipses. Fig. 4 shows three of the clearest individual egresses (in general the others have lower S/N, or are harder to interpret owing to greater source variability just after, and presumably in, egress). It is immediately clear that the egress occurs at different phases in the different eclipses. Thus, let's consider the phase shifts we expect in the simplest case.

Fig. 5 illustrates the white dwarf emerging from eclipse. An accretion region (spot) moves along a track of constant latitude as the white dwarf rotates. At such a high inclination the accretion region will only be in view for half the spin cycle, spending the other half behind the white dwarf. The fact that the quiescent spin pulse has a low amplitude (Sections 2 & 6) implies that we must see accretion regions at both poles of a roughly symmetric dipolar field, so that the appearance of one pole compensates for the disappearance of the other. Thus the accretion region at the upper pole comes over the limb into view at spin phase 0.25, travels across the face of the white dwarf, and disappears at phase 0.75; also at phase 0.75, the accretion region at the lower pole comes into view and travels across the white dwarf, before disappearing at phase 0.25. Of course the chosen phase zero point is arbitrary, but reflects the convention that phase zero is taken as the maximum of the spin pulse, and my prejudice that in IPs this typically occurs when the upper pole points away from the observer.

The above assumes that the height of the accretion regions above the white dwarf surface is negligible, a point to which I return in Section 5. Fig. 5 also contains two simplifications which are unimportant compared to other uncertainties, but which make the egress times amenable to simple geometry. I have assumed that the limb of the secondary is straight (at a constant angle from the vertical of θ) rather than curved; and similarly that the inclination is sufficiently high that a line of constant latitude projected onto the plane of the sky can be taken as straight, rather than slightly curved.

To measure the egress times in the individual lightcurves I first tried a generalisation of the fitting procedure described for the averaged profile. This modelled the un-eclipsed light with sinusoids at the spin period and its first harmonic, and multiplied this by the linear cutoff during egress. However, the flickering and cycle-to-cycle variability in the lightcurves is large, and this can lead to a bias when the fitting code lengthens the egress to model brightenings occurring after egress. I therefore turned to a different method of measuring 3rd contact, which proved to be more robust. This simply stepped through the lightcurve starting in eclipse, calculated the χ_ν^2 about zero flux of the data so far, and recorded the time at which the χ_ν^2 rises significantly. By this method I arrived at the 19 times of 3rd
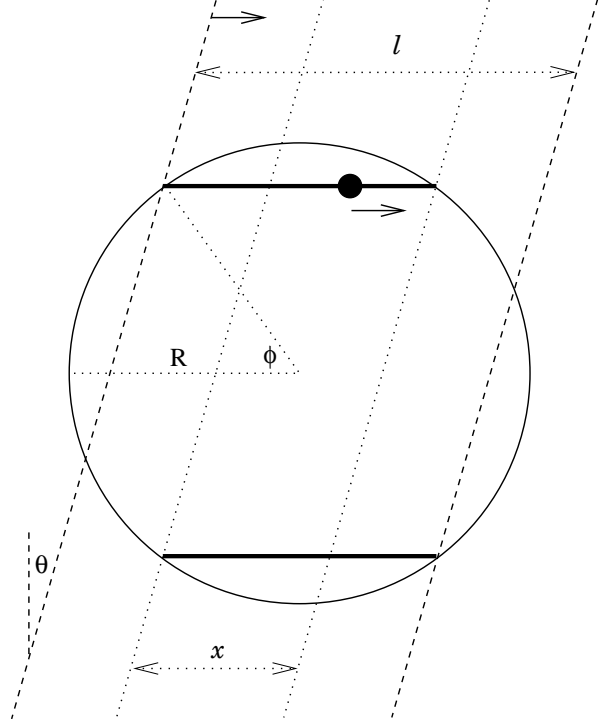

Figure 5. An illustration of the egress of the white dwarf as the secondary star limb moves from left to right. It assumes that X-ray emission comes only from regions of fixed latitude ϕ. θ is the angle of the secondary star limb, R the radius of the white dwarf and l the motion of the limb between 3rd and 4th contact in spin-averaged data.

contact plotted in Fig. 6 (one eclipse was discarded owing to a data drop-out during egress).

Fig. 6 shows a clear trend to later eclipse times with later spin phase (as expected if the white dwarf rotates in the same sense as the binary, as it almost certainly must). The earliest eclipse times occur when the upper pole has just come over the limb, and, as discussed above, I have adjusted the phasing in Fig. 6 so that this occurs at spin phase 0.25. Half a cycle later, when the upper pole disappears and the lower pole appears, the contact times jump earlier. The dashed lines illustrate the expected change in contact phase over the spin cycle, following the geometry in Fig. 5 (the track for each pole is sinusoidal since it is the transverse component of the motion which affects the phase of contact). The two free parameters affecting the tracks (their total phase span, corresponding to l in Fig. 5, and their separation at phase 0.75, corresponding to x) were adjusted to match the data. The total phase span of 3rd contact times is 22 ± 2 s, compatible within the errors with the egress length of the averaged lightcurve, which provides a check on the correctness of the procedure so far.

The one aberrant point in Fig. 6 (plotted as a triangle) occurred at the peak of the outburst, and is discussed further in Hellier et al. (1997). The second-brightest outburst observation was the point omitted because of a data drop-out. The remaining outburst points all occur close to quiescent points having the same spin phase, so the plot would not change significantly if only quiescent points were included.
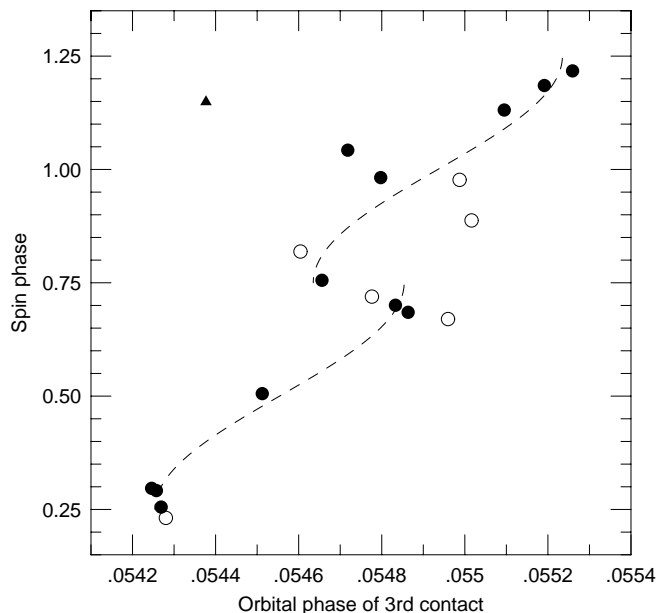
Figure 6. The orbital phases of 3$^{\rm rd}$ contact for each egress, against the spin phase at which 3$^{\rm rd}$ contact occurred. The unfilled symbols indicate lightcurves which are less reliable because of a lower count rate. The discrepant point plotted as a triangle occurred at the peak of the outburst. The uncertainties in orbital phase are typically 5×10^{-5}, or up to 2×10^{-4} for unfilled points. The dashed lines show the expected track of a point on the white dwarf (see text). The total phase span of the dashed lines corresponds to the length l in Fig. 5, while their separation at phase 0.75 corresponds to x.

4   THE LOCATION OF THE ACCRETION REGIONS

In order to translate the egress times in Fig. 6 to locations on the white dwarf we need to review the geometry of the binary. From ellipsoidal modelling of the IR lightcurve Allan et al. (1996) limit the mass ratio to $0.4 < q < 0.7$ and the inclination to $80° < i < 87$. We can also use the fact that the secondary fills the Roche lobe of the 6.06-h binary, together with a mass–radius relation (e.g. Patterson 1984; Warner 1995), to estimate the secondary mass as 0.62 M$_\odot$. Together with the limits on q this implies a white dwarf mass of ~ 1 M$_\odot$.

As mentioned above, though, both the distribution of points in Fig. 6 and the fact that the spin pulse has a low amplitude suggest that we are seeing both poles of the white dwarf. This further restricts the inclination, as shown by the following. Accretion will be inhibited by a centrifugal barrier if the velocity of the field lines at the point of disc disruption exceeds the local Keplerian velocity. Assuming that they are the same, the 206-s spin period and 1 M$_\odot$ white dwarf mass locate the inner radius of the disc at 5.2×10^9 cm, compared to a white dwarf radius of 5.6×10^8 cm. This implies that the inclination must be no higher than 84° in order to see the bottom of the white dwarf, even assuming that the disc has zero thickness at the disruption point.

I therefore proceed with the range $80° < i < 84°$. The length of the X-ray eclipse (2050 s; Kamata et al. 1991; Allan et al. 1996) then fixes the mass ratio to $0.48 < q < 0.68$, using

figure 2 of Horne (1985). For these values of q and i the angle of the secondary star limb at the white dwarf (θ in Fig. 5) ranges from 20° ($i=84°$) to 30° ($i=80°$).

From the geometry illustrated in Fig. 5 one can show that

$$\frac{l}{2R} = \frac{\cos(\theta - \phi)}{\cos\theta}$$

and

$$\frac{x}{2R} = \frac{\cos(\theta + \phi)}{\cos\theta}$$

and hence

$$\frac{x}{l} = \frac{\cos(\theta + \phi)}{\cos(\theta - \phi)}.$$

The ratio x/l can be gained from Fig. 6; a formal fit to the plotted tracks yields $x/l = 0.22 \pm 0.06$. Hence, including the uncertainty in θ, the latitude of the accretion regions, ϕ, lies in the range 44° to 63°. Further, the ratio R/l will be 0.45–0.64 (at the lower end of the range for $\theta = 30$ and the upper end for $\theta = 20$).

To translate $l = 25^{+1.5}_{-1.8}$ s into a length we need the orbital speed of the secondary star with respect to the white dwarf. From Kepler's law,

$$v^3 = \frac{2\pi G (M_1 + M_2)}{P},$$

where v is the velocity and P the orbital period. Assuming M$_2$ = 0.62 M$_\odot$, the velocity is between 390 km s^{-1} ($q=0.68$) and 420 km s^{-1} ($q=0.48$). Hence we finally arrive at a white dwarf radius in the range 4.3–7.3 $\times 10^8$ cm. Using the Hamada & Salpeter (1961) mass-radius relation for a white dwarf, but increasing the radius by 5 per cent following the work of Koester & Schoenberner (1986), this translates to a mass in the range 0.78–1.17 M$_\odot$.

The limits on the white dwarf mass are not much different from those given by the range of q and the assumed secondary star mass-radius relation (0.91–1.29 M$_\odot$); however the consistency does suggest that the procedure so far, and the interpretation of Fig. 6, is essentially correct. Thus, to sum up, the accretion regions are seen at both poles, lying at a latitude between 44° and 63°, on a white dwarf whose diameter is a length translating to between 22 and 35 s of secondary star motion.

5   THE SIZE OF THE ACCRETION REGION

Again, before seeing what the data say about the size and shape of the accretion region, let's review the standard picture of what we expect. The magnetic field will pick up material from the inner edge of the disc and channel it along field lines onto the white dwarf. The range of azimuth in the disc translates, with sufficient accuracy for present purposes, to a ring of constant magnetic latitude around the magnetic pole (see, e.g., Rosen et al. 1988; Kim & Beuermann 1995). If the disc is disrupted at a radius of ~ 9 R$_{\rm wd}$, as suggested in Section 4, the magnetic colatitude of this ring, ϵ, will be $\sim 19°$. The magnetic axis will be offset from the orbital plane by an angle δ (otherwise there would be no spin pulse) so we expect a variation in accretion rate with azimuth such that most accretion arrives from the azimuth to which the magnetic pole points, translating to a
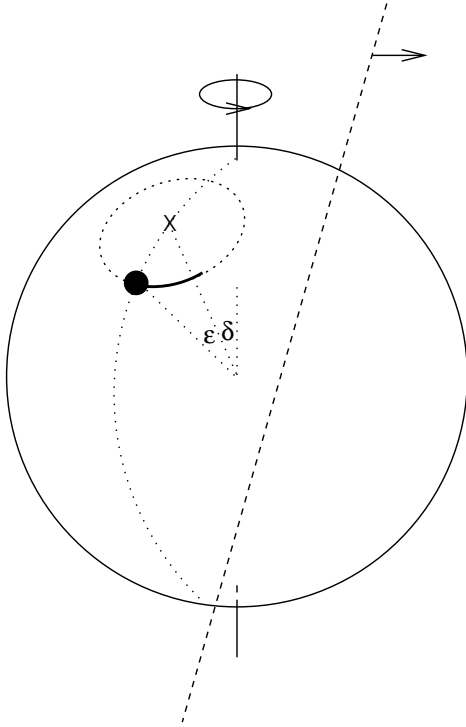
Figure 7. An illustration of the expected accretion regions in a magnetic accretor. The magnetic pole, X, is offset from the spin axis by an angle δ. The accretion regions lie approximately on a circle of constant magnetic latitude, at a further angle ϵ from the magnetic pole. The highest accretion rate is expected furthest from the spin axis. As the white dwarf spins this point moves along a line of constant latitude, as shown in Fig. 5.

location on the ring around the magnetic pole directly opposite the spin axis (Fig. 7). The accretion rate would fall off in either direction along the ring, producing arc shaped accretion regions extended along lines of constant magnetic latitude. From the previous section we have the constraint that $\epsilon + \delta = 90 - \phi$, where ϕ lies in the range 44–63°. With $\epsilon \sim 19°$ this implies $8° < \delta < 27°$.

Turning to the data, one could investigate the size of the accretion region either by looking at individual eclipses, or by summing the eclipses, shifting them in phase to account for their different locations on the white dwarf. The first method suffers from low S/N while the second is risky, since if the phase adjustments are wrong the result will be artificially smeared out.

Pursuing the second method, Fig. 8 shows the egress formed by combining the eclipses while subtracting from each the phase of its location on Fig. 6 (for this and the following results I omitted the two eclipses at the outburst peak). Two thirds of the flux emerges in <2 s while the remaining third emerges more slowly, so that the whole egress lasts ~ 20 s. Could the <2 s egress be an artefact of lining up flickers in individual eclipses? To some extent it could, but if the flickers were photon noise one could only line up individual bins, and would expect the subsequent bins to revert to the average trend. The fact that there is no decrease after the rapid egress shows that it cannot be photon noise. Similarly the rapid egress is unlikely to be an artefact of source flickering, since this would imply that 18 eclipses had con-

spired to show excess light through flickering at exactly the moment the accretion regions began to be uncovered. Further, under the hypothesis that the true egress were slower, most of the accretion region would still be hidden at the beginning of egress. It is implausible that the small region visible could, on its own, produce flickers of $2/3^{\rm rds}$ the intensity of the entire region.

The slower, ~ 20 s, egress is more plausibly an artefact, since if any of the eclipses had the wrong phase correction, again possibly through flickering, a smeared egress would result. Again, though, flickering is least likely to be a factor in measuring $3^{\rm rd}$ contact, and a careful examination suggested that the slower section of the egress is real.

In contrast to the 'empirically' corrected egress in Fig. 8, Fig. 9 shows the combined egress, this time subtracting the phase of the dashed lines in Fig. 6, appropriate for the spin phase of the egress. For comparison the uncorrected egress from Fig. 3 and the empirically corrected egress are shown again. The egress using the calculated corrections is faster than the uncorrected egress, with $2/3^{\rm rds}$ of the flux emerging in ~ 5 s, but it is slower than the empirically corrected egress.

My interpretation of Figs. 8 & 9 is as follows: the majority of the X-rays ($\sim 2/3^{\rm rds}$) emerge, at any one time, from a very small region (< 2 s), located at the trailing edge of the accretion region. The remainder of the flux arises from a much more extended region which leads the small, bright region, and produces the slower part of the egress.

Further, the location of the bright region is not determined solely by spin phase, but can deviate from its spin-averaged location by up to ~ 2 s, so that lining up the eclipses using spin phase only, rather than the empirical position, smears the bright spot over a larger region.

Having interpreted the summed egress from all the eclipses, I have checked for consistency with the individual egresses. Because of the low S/N these only give upper limits on the egress times. The three eclipses in Fig. 4 give upper limits of (from top to bottom) 9, 4 & 5 s (68 per cent confidence) or 11, 10, 15 s (90 per cent confidence). The other eclipses gave weaker limits. Thus all the individual eclipses are consistent with a rapid egress in 2-s, but their low S/N limits their usefulness. The slower part of the egress is not traceable in the individual lightcurves.

5.1 Complicating factors

There are several complications to be considered before translating the measured times into sizes on the white dwarf.

(i) If the secondary limb is not a sharp edge the transitions will be lengthened. This, though, simply makes the above upper limits firmer. The egress time of <2 s implies that the secondary edge is sharp to 800 km, or $\Delta r/r \lesssim 2\times10^{-3}$. The hard X-rays will be stopped by a column $> 10^{24}$ cm^{-2}, while the path length through the secondary limb will be $\sim 10^{10}$ cm, implying that the secondary edge occurs at a density of $\sim 10^{14}$ cm^{-3}. This will be located in the chromosphere at a point where the density increases by an order of magnitude over a vertical distance of 300 km (e.g. Withbroe & Noyes 1977). Thus, fuzziness of the secondary star becomes important at about the 1 s level.

A similar consideration is that if the atmosphere of the secondary changes, because of sunspots for instance, so that
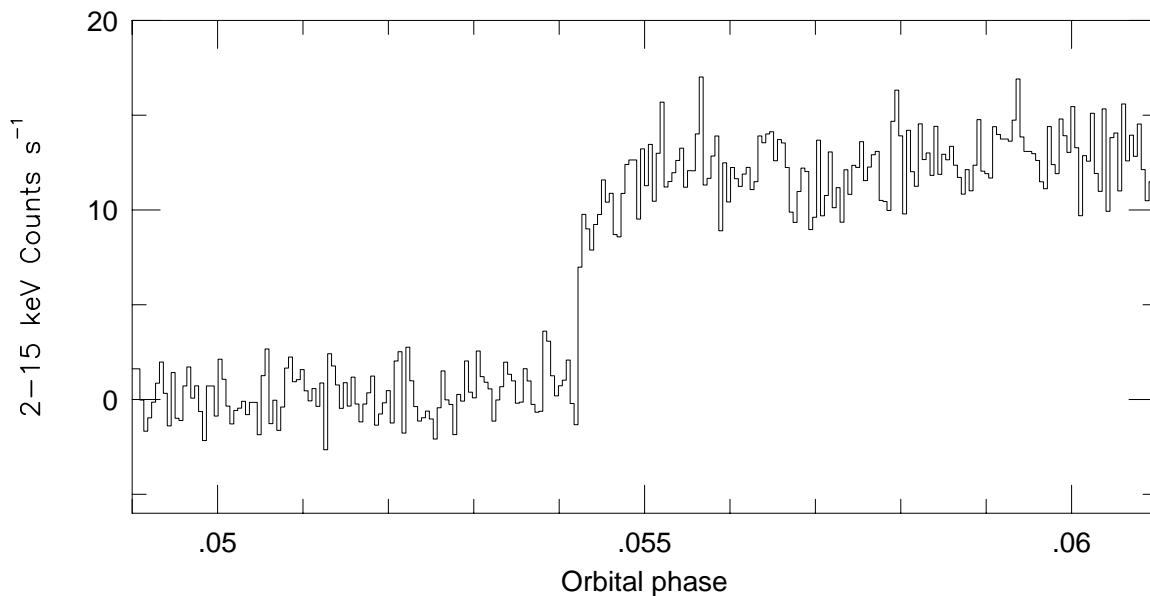
Figure 8. The average eclipse egress using an empirical phase correction (see text). Each bin lasts 1 s.

the location of the edge varies by $\Delta r/r \lesssim 2 \times 10^{-3}$, it could explain some of the apparent phase wandering seen when lining up the eclipses using the spin phase only.

(ii) Many of the X-ray photons will be scattered into a halo as they pass through the molecular cloud Lynds 1457. Mauche & Gorenstein (1986) find that for GX 13+1 and Cyg X-3, with columns of 5×10^{22} and 3×10^{22} cm^{-2} respectively, the halo contains 0.19 and 0.33 of the total intensity at an energy of 2.4 keV. XY Ari has a somewhat larger column of 8×10^{22} cm^{-2}; however the 2–15 keV pass band will give a higher flux-weighted mean energy, E, of 6 keV, and the scattering cross-section decreases as E^{-2}. Thus we would expect 5–15 per cent of the photons to be scattered.

The time delay caused by the longer path length can be estimated using (e.g. Bode et al. 1985)

$$\Delta t \approx 0.22 \left(\frac{a}{0.25\mu\mathrm{m}} \right)^{-2} \left(\frac{E}{1\,\mathrm{keV}} \right)^{-2} \left(\frac{D}{2.5\mathrm{kpc}} \right) \mathrm{days}.$$

For a grain size, a, of 0.1 μm, an energy of 6 keV, and a source distance, D, of 300 pc, this gives a delay of ~ 400 s.

The two estimates suggest that the halo is somewhat too weak and varying too slowly to cause the slower part of the observed egress (one third of the flux emerging in 20 s), although it could become important in higher S/N data. Halo photons could also explain the excess of photons in mid-eclipse above the estimated background (Section 2).

(iii) The calculations so far have assumed that the shock height above the white dwarf surface can be neglected. Standard theory (e.g. Frank, King & Raine 1992) yields an upper limit to the shock height given by

$$D \sim 9 \times 10^9 \dot{M}_{17}^{-1} f M_1^{3/2} R_9^{1/2} \mathrm{cm}$$

where $\dot{M}_{17}^{-1}$ is the accretion rate in 10^{17} g s^{-1}, which can be taken as ~ 1 for an IP above the period gap (e.g. Patterson 1994); M_1 is the primary mass in solar units, which from above is ~ 1; R_9 is the white dwarf radius in 10^9 cm, which is ~ 0.55; and f is the accretion area as a fraction of the white dwarf.

Assuming that the bright spot is circular with a diameter of 2 s, and that the white dwarf is spherical with a diameter of at least 22 s, we have $f < 0.002$. This gives $D < 0.02 R_{\mathrm{wd}}$ and justifies the assumption of negligible height. However, for the extended region, f could be 0.1, and since the extended region emits $\sim 1/3^{\mathrm{rd}}$ of the flux, its share of $\dot{M}$ could be $\sim 1/6^{\mathrm{th}}$ per pole, implying $D \sim R_{\mathrm{wd}}$. This means that the extended region could have a large height, rather than a large area, even though the emission from an accretion column will emerge largely from the higher density base of the column. However, the fact that none of the slower egress precedes the rapid egress suggests that it does not have a significant height, since this would cause it to egress earlier when the upper pole is emerging over the limb.

(iv) The aspect of the accretion region presented to the white dwarf limb can change. The egress, of course, is only sensitive to the extent of the region in a direction perpendicular to the limb. Fortunately, if we suppose that the accretion region's shape is fixed relative to the magnetic field, the orientation of the region will change as the white dwarf spins. Thus, since the summed egress samples 18 different spin phases, the result will approximate to an averaged cut across the region, especially since the egresses sample both poles, which will also have different orientations. Nevertheless, this effect should be borne in mind and a correction factor, either reducing or increasing the size of the region, could be applied given greater knowledge of the shape of the region.

It is also possible, in principle, that the rapid and slower parts of the egress arise from one region which is extended into a long ribbon, giving both slow and rapid egresses depending on its aspect. However, since the most likely extension is along lines of constant magnetic latitude, this would lead to longer egresses soon after white dwarf 3$^{\mathrm{rd}}$ contact and shortly before white dwarf 4$^{\mathrm{th}}$ contact, with shorter egresses in between (see Fig. 7). The data, though, show no such effect, with rapid egresses occurring at all spin phases, suggesting that the small bright spot is real. Note, though,
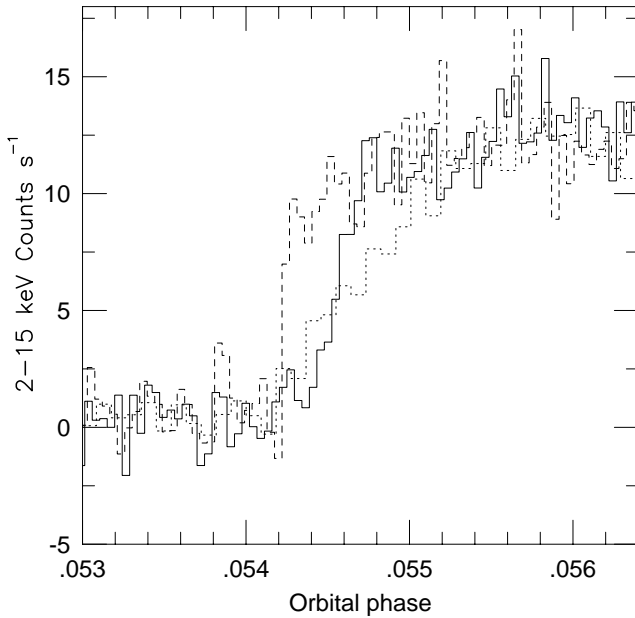
Figure 9. The average eclipse egress using a phase correction calculated from the spin phase alone (see text). Each bin lasts 1 s. For comparison the dashed line shows the empirically corrected egress and the dotted line the uncorrected egress.

that this conclusion would be more robust if the individual egresses had a higher S/N. In particular the slower egress is only discernable in the summed egress and can't be investigated as a function of spin phase.

A similar complication is that if the accretion regions have a negligible shock height they will appear foreshortened when on the white dwarf limb, in a direction perpendicular to the limb. However, while the angle between the direction of foreshortening and the direction perpendicular to the secondary limb can be low during the appearance of the upper pole ($\phi - \theta$, in the nomenclature of Fig. 5) it will be larger at the disappearance of the pole ($\phi + \theta$; and similarly in reverse for the lower pole). Thus, when averaged over all egresses, including many not near the limb, foreshortening will have a minor effect.

(v) The accretion regions are themselves moving with the white dwarf rotation. The white dwarf radius of 4.3–7.0 $\times 10^8$ cm and spin period of 206 s imply an equatorial surface motion of 130–210 $\mathrm{km\,s^{-1}}$. For an accretion region at the equator in the middle of the white dwarf the effective speed of the secondary is reduced by this amount, although the effect dies away sinusoidally in moving towards the pole or towards the limb, so that again the effect on the averaged egress will be minor. Since the correction to the averaged egress for this effect will be in the opposite sense to the effect of foreshortening, and since neither can be calculated securely given the uncertainties in the locations of the regions on the white dwarf, it is easier to make neither correction.

5.2   The value of f

Bearing in mind the above complications, let's move to the value of f. The rapid egress of $2/3^{\mathrm{rds}}$ of the X-ray flux occurs

in <2 s. Assuming a circular region with this value as the diameter is also likely to be an upper limit, since the accretion region is likely to be arc-shaped and so have a smaller area. Thus, taking the smallest white dwarf diameter of 22 s (to again give an upper limit), we obtain $f < 0.002$ for each pole. This is the area over which the bulk of the accretion is occurring at any one time; f_{acc} in the terminology of King (1995).

Recall, though, that the accretion spot appears to wander from its mean position, so that $2/3^{\mathrm{rds}}$ of the flux emerges in 5 s in the spin-phase corrected egress. This leads to $f_{\mathrm{zone}} < 0.01$ per pole, for the fractional area over which accretion can occur. Again this is likely to be an upper limit since, whatever mechanism causes the wandering, it is likely to occur preferentially along either magnetic latitude or longitude (and we can't rule out changes in the secondary star as the cause).

Finally, there is the remaining $1/3^{\mathrm{rd}}$ of the flux which appears to emerge from a more extended region, having an egress time comparable with the white dwarf radius (although I repeat that higher S/N data are required to confirm its existence, since it could be an artifact of incorrect phase correction). It is also harder to translate this into a value for f. Firstly, it is hard to disentangle a higher shock height from a larger f, although as remarked previously, the fact that none of the slower egress appears to precede third contact with the white dwarf suggests that a higher shock is not an important factor. Secondly, the most likely explanation of an egress time comparable with the size of the white dwarf is accretion regions visible at both magnetic poles simultaneously, since they will be separated by a white dwarf diameter. If there is any significant extension of the accretion arcs then parts of both will be visible when they are on the limb, and the greater their extent the greater the range of spin phases over which parts of both accretion regions are visible. However, it is also possible that the slower egress does imply a greatly extended emission region. If so, the summed egress gives knowledge of one dimension, but not of the others. If we assume $f \sim 0.1$ we find an estimated brightness, or flux per area, of $1/100^{\mathrm{th}}$ that of the bright spot. Distinguishing between these possibilities will need higher S/N data capable of tracing the slower egress in individual eclipses.

6   THE SPIN PULSE

I show the quiescent data folded on the spin period in Fig. 10, together with the 6–15/2–5 keV hardness ratio (the spin pulse in outburst is discussed in Hellier et al. 1997). Both the double-peaked profile and the hardness ratio changes are similar to those in the *Ginga* data reported by Kamata & Koyama (1993). The phasing in Fig. 10 corresponds to that in Fig. 6, so that the upper pole emerges over the white dwarf limb at phase 0.25.

As previously mentioned, the amplitude of the spin pulse is much lower than in IPs such as AO Psc, which has an ~ 80 per cent pulse (e.g. Hellier et al. 1996). Thus the appearance of one pole over the limb must compensate for the disappearance of the other pole. In a symmetric situation with negligible shock heights this would lead to no spin pulse. The low amplitude, double-peaked pulse in XY Ari
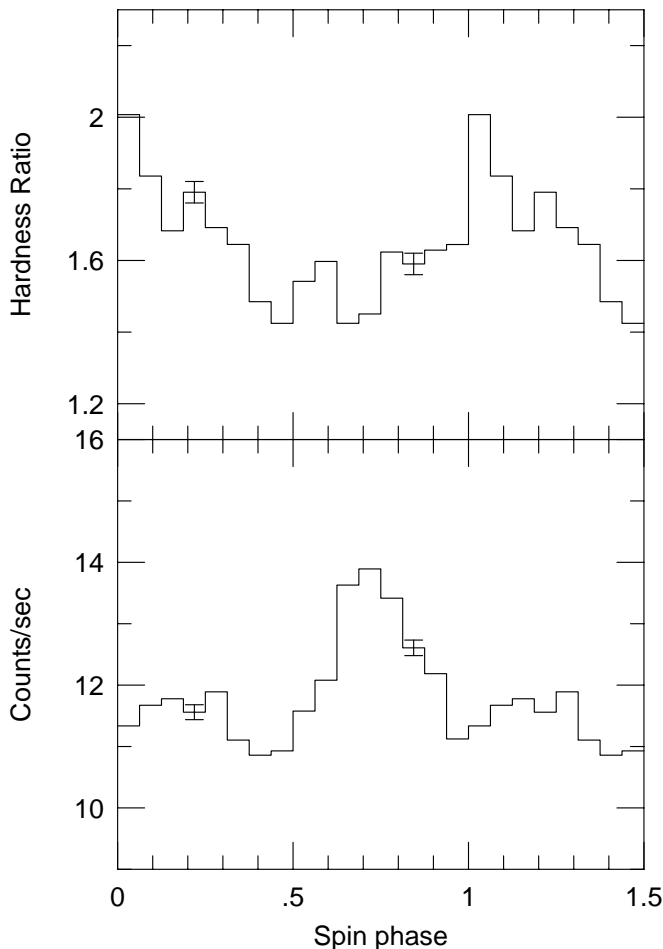
Figure 10. The data from all 20 observations folded on the spin period, together with the 6–15/2–5 keV hardness ratio. The phasing is the same as in Fig. 6, and is chosen so that the upper pole appears over the white dwarf limb at phase 0.25. Phase 1 occurs at TDB 245 0277.40382

Table 1. System parameters of XY Ari

Orbital period	21832.990(5)	secs
Spin period	206.298(5)	secs
Inclination, i	80–84	degrees
Mass ratio, q	0.48–0.68	
White dwarf radius	4.3–7.0×10^8	cm
White dwarf mass	0.91–1.17	$M_\odot$
Red dwarf mass	~ 0.62	$M_\odot$
Inner disc radius	~ 9	$R_{\rm wd}$
Latitude of accretion, ϕ	44–63	degrees
Magnetic colatitude of accretion, ϵ	19	degrees
Magnetic dipole offset, δ	8–27	degrees
Accretion area, $f_{\rm acc}$	< 0.002	
Range of accretion area, $f_{\rm zone}$	< 0.01	

encounter far more absorption than the line of sight to the upper pole, which can explain the different behaviour.

7 DISCUSSION

The essential result of this paper is that the majority of the X-ray flux emerges, at any one time, from regions covering < 0.002 of the white dwarf surface at each pole. These regions, however, wander in location, covering an area of < 0.01 of the white dwarf. Further, there is evidence that either we can often see some flux from both poles simultaneously, or that a minority of the X-ray flux emerges from a much more extended region, probably preceding the bright region in phase. Note that these results derive from quiescent observations. In Hellier et al. (1997) we deduce that the accretion regions become much more extended in outburst.

There are only a few other estimates of the accretion area in IPs for comparison. Hellier (1993) argued that the upper pole in FO Aqr must have $f \sim 0.001$, but this was from a model-dependent interpretation of the spin pulse. Also, some of the IPs discovered with *Rosat* show strong blackbody emission, presumably from the heated pole-cap. Haberl et al. (1995) use this to estimate $f \sim 10^{-5}$ for RX 0558+53 for a distance of 300 pc, although as usual the distance is suspect. Similarly, the polarised light from PQ Gem allows an estimate of the area emitting cyclotron radiation, and Vath, Chanmugham & Frank (1996) model the emission to find $f_{\rm cyc} \sim 0.006$. Further, values of $f \sim 0.01$–0.001 are expected using current (but highly uncertain) theoretical expectations for the magnetic disruption of a disc (e.g. Rosen 1992).

In AM Her stars many more estimates are available from the blackbody radiation, from cyclotron emission, and from eclipses. Typical values are $f_{\rm cyc} \sim 3 \times 10^{-4}$, $f_{\rm bb} \sim 10^{-5} - 10^{-6}$ (e.g. Stockman 1995) and, from eclipses of UZ For, $f_{\rm acc} < 0.005$ (Bailey & Cropper 1991).

Thus all values are consistent and suggest that polecap areas have f of order 10^{-3} in IPs and are even smaller in AM Her stars. The larger f in IPs is expected since an accretion disc can feed accretion over a larger range of azimuth than a stream will.

One consequence of this is that occultation of such regions will produce sharp features in the X-ray spin-pulse profiles (barring special grazing geometries) and so can explain features such as the 'notch' in the spin pulse of FO Aqr. The much broader quasi-sinusoidal modulations typical of

can then be attributed to asymmetries between the poles, or the effect of a non-negligible shock height for at least some of the X-ray flux.

At phase 0.25 in Fig. 10 the flux starts to decline. Since this is when the lower pole disappears and the upper pole appears, it suggests that the lower pole is slightly brighter. The maximum flux is seen half a cycle later, near phase 0.75, when the lower pole would be appearing and the upper pole disappearing. It is possible that they aren't directly opposite each other so that more of both regions is visible for a short time, producing extra flux. Being more specific is hard without a greater knowledge of the shape and extent of the accretion regions.

The hardness ratio is greater in the phase range 0.75–0.25, when the flux comes from the lower pole. Normally, this would argue against the accretion curtain model for the spin modulation, which proposes that greater absorption, and hence a harder spectrum, would be expected when the upper pole points towards us (e.g. Hellier et al. 1996). However, as shown in Section 4, the inclination of XY Ari is so high that the line of sight to the lower pole skims over the inner edge of the disc. It is therefore likely that this line of sight will

IPs must be caused by absorption, which fits with their characteristic greater depth at lower energies. The high spectral resolution of *ASCA* data confirms this at least in the case of AO Psc (Hellier et al. 1996).

The small accretion areas also imply very high densities in the accretion column. Rosen (1992) shows that this will produce substantial electron scattering, and so, by beaming the X-ray flux from the column, spin-modulate the X-rays even at high energies. This, in turn, implies that the material must be highly ionized (as expected in the post-shock region) or otherwise an inefficient absorber, in order for any low energy X-ray flux to be seen at spin minimum.

Despite the above, though, absorption seems to contribute little to the spin pulse in XY Ari. Instead, the low-amplitude, complex, double-peaked pulse appears to result from asymmetries between the accretion regions at the two magnetic poles, so that occultation effects do not entirely cancel. Why the difference between it and AO Psc? One reason is that XY Ari is already hidden behind a column of 10^{23} H atom cm^{-2}, provided by the molecular cloud, so that changes in more tenuous absorbers will have little effect. In AO Psc we found that the absorber consisted of several phases: a dense 2×10^{23} column, associated with the flow very near the white dwarf, immediately before the accretion shock; and a less dense leaky absorber of 2×10^{22}, associated with parts of the accretion flow far from the white dwarf, possibly where the magnetically channelled material rises above the plane of the accretion disc.

Thus, a possible resolution involves the higher inclination of XY Ari. Looking virtually along the plane of the binary, with the accretion columns falling onto the magnetic poles of the binary at an angle of between 43° and 63° to the plane, the denser pre-shock material would never obscure the line of sight. Thus the only absorption in XY Ari would result from the material rising out of the plane near the magnetosphere, and if this had a similar density to that in AO Psc it would be unnoticeable given the greater column of the molecular cloud. In the lower inclination AO Psc ($i \sim 60°$) the pre-shock material would cross the line of sight, and so cause the very deep, absorption-induced spin pulse.

It is notable that the other eclipsing IP, EX Hya, also has a spin pulse showing very little sign of absorption (e.g. Ishida, Mukai & Osborne 1994; Allan, Hellier & Beardmore 1997). Probably the high inclination reduces the effect of absorption in this star also. [Ironically, despite the fact that the accretion curtain model was first developed for EX Hya, it now appears that it applies far better to stars such as AO Psc and does not explain the X-ray behaviour of EX Hya.]

Although the data show that the accretion area, $f_{\rm acc}$, is < 0.002 at any one time, the area over which the accretion wanders, $f_{\rm zone}$, is larger at < 0.01. Since the eclipses are distributed over a month and are typically separated by 1 day, we can't tell whether the wandering occurs from spin cycle to spin cycle, or on a timescale of days. Presumably the wandering reflects fluctuations in the connection of the field lines onto the inner disc, and if this takes place on short timescales it might explain much of the flickering in this and other IPs.

The existence of a slower section of egress in addition to the rapid egress is a sign of structure in the accretion region. If it is caused by viewing emission from both poles simulta-

neously it implies that accretion occurs along an extended arc around each magnetic pole, and hence that each pole receives at least some material from a range of azimuths. The different angle of the field lines to the disc at different azimuths would then modulate the rate of accretion with azimuth to produce much more intense emission at one location on the ring, and thus the bright spot responsible for the rapid egress.

If, instead, the accretion regions at the pole disappear completely behind the white dwarf, the slower egress implies a large but faint extension to the bright spot. The current egresses have too low a S/N to trace this feature in individual egresses, so further investigation will have to await future satellites. However, the fact that the slower egress occurs largely after the rapid egress implies that the faint extension leads the bright spot on the white dwarf, suggesting that field lines ahead of direction in which the magnetic axis points accrete preferentially compared to those behind. Interestingly a similar asymmetry has recently been suggested for PQ Gem, based on X-ray data (Mason 1997), optical spectroscopy (Hellier 1997) and polarimetry (Potter et al. 1997). Thus we seem to be accumulating the first observational clues to the structure of the interaction between the magnetic field and the inner disc.

8   CONCLUSIONS

(1) The majority of the X-ray flux emerges from eclipse in < 2 s, implying that the accretion polecaps have areas of < 0.002 as a fraction of the white dwarf surface.

(2) The accretion footprints are not fixed in position on the white dwarf, but can wander over an area < 0.01 of the white dwarf surface.

(3) There is evidence that a minority of the flux arises from a much larger area, or that we can always see part of the accretion regions at both poles.

(4) The accretion regions are at a latitude in the range 43°–63°, which suggests a magnetic dipole offset of 8°–27° (constraints on other system parameters are listed in Table 1).

(5) We see roughly equal amounts of X-ray flux from both upper and lower poles. There are, though, slight asymmetries so that the disappearance of one pole over the white dwarf limb does not entirely compensate for the appearance of the other pole. The net effect is a low-amplitude, complex spin pulse.

REFERENCES

Allan A., Hellier C., Ramseyer T. F., 1996, MNRAS, 282, 699
Allan A., Hellier C., Beardmore, A. P., 1997, in preparation
Bailey J., Cropper M., 1991, MNRAS, 253, 27
Bode M. F., Priedhorsky W. C., Norwell G. A., Evans A., 1985, ApJ, 299, 845

Bradt H. V., Rothschild R. E., Swank J. H., 1993, A&AS, 97, 355

Frank J., King A. R., Raine D. J., 1992, Accretion power in astrophysics, Cambridge University Press, Cambridge

Haberl F., Thorstensen J. R., Motch C., Schwarzenberg-Czerny A., Pakull M., Shambrook A., Pietsch W., 1994, A&A, 291, 171

Hamada T., Salpeter E. E., 1961, ApJ., 134, 683

Hellier C., 1993, MNRAS, 265, L35

Hellier C., 1995, in Buckley D.A.H., Warner B., eds, Cape workshop on magnetic cataclysmic variables, ASP Conf series, 85, 185

Hellier C., 1997, MNRAS, in press

Hellier C., Cropper M., Mason K.O., 1991, MNRAS, 248, 233

Hellier C., Mukai K., Ishida M., Fujimoto R., 1996, MNRAS, 280, 877

Hellier C., Mukai K., Beardmore A. P., 1997, MNRAS, submitted

Horne K., 1985, MNRAS, 213, 129

Ishida M., Mukai K., Osborne J., 1994, PASJ, 46, L81

Kamata Y., Tawara Y., Koyama K., 1991, ApJ, 379, L65

Kamata Y., Koyama K., 1993, ApJ, 405, 307

Kim Y., Beuermann K., 1995, A&A, 298, 165

King A. R., 1995, in Buckley D.A.H., Warner B., eds, Cape workshop on magnetic cataclysmic variables, ASP Conf series, 85, 21

King A. R., Shaviv G., 1984, MNRAS, 211, 883

Koester D., Schonberner D., 1986, A&A, 154, 125

Mason K. O., 1997, MNRAS, in press

Mauche C. W., Gorenstein P., 1986, ApJ, 302, 371

Norton A. J., Watson M. G., 1989, MNRAS, 237, 853

Patterson J., 1984, ApJS, 54, 443

Patterson J., 1994, PASP, 106, 209

Patterson J., Halpern J. P., 1990, ApJ, 361, 173

Potter S. B., Cropper M., Mason K. O., Hough J. H., Bailey J. A., 1997, MNRAS, 285, 82

Rosen S. R., 1992, MNRAS, 254, 493

Rosen S. R., Mason K. O., Cordova F. A., 1988, MNRAS, 231, 549

Stockman H. S., 1995, in Buckley D.A.H., Warner B., eds, Cape workshop on magnetic cataclysmic variables, ASP Conf series, 85, 153

Vath H., Chanmugam G., Frank J., 1996, ApJ, 457, 407

Warner B., 1995, Cataclysmic variables, Cambridge University Press, Cambridge

Withbroe G. L., Noyes R. W., 1977, ARA&A, 15, 363

Zuckerman B., Becklin E. E., McLean I. S., Patterson J., 1992, ApJ, 400, 665